Reactive Semiconductor Nanocrystals for Chemoselective Biolabeling and Multiplexed Analysis

Travis L. Jennings,[†,*] Sara G. Becker-Catania,[†] Robert C. Triulzi,[†] Guoliang Tao,[†] Bradley Scott,[†] Kim E. Sapsford,[‡] Samantha Spindel,[‡] Eunkeu Oh,[§] Vaibhav Jain,[§] James. B. Delehanty,[⊥] Duane E. Prasuhn,[⊥] Kelly Boeneman,[⊥] W. Russ Algar,[⊥,∥] and Igor L. Medintz[⊥,*]

[†]eBioscience, Inc., 10255 Science Center Drive, San Diego, California 92121, United States, [‡]Division of Biology, Science and Engineering Laboratories, U.S. Food and Drug Administration, Silver Spring, Maryland 20993, United States, [§]Optical Sciences Division, Code 5611, and [⊥]Center for Bio/Molecular Science and Engineering, Code 6900, U.S. Naval Research Laboratory, 4555 Overlook Avenue, S.W., Washington, D.C. 20375, United States, and [∥]College of Science, George Mason University, Fairfax, Virginia 22030, United States

ABSTRACT Effective biological application of nanocrystalline semiconductor quantum dots continues to be hampered by the lack of easily implemented and widely applicable labeling chemistries. Here, we introduce two new orthogonal nanocrystal bioconjugation chemistries that overcome many of the labeling issues associated with currently utilized approaches. These chemistries specifically target either (1) the ubiquitous amines found on proteins or (2) thiols present in either antibody hinge regions or recombinantly introduced into other proteins to facilitate site-specific labeling. The amine chemistry incorporates aniline-catalyzed hydrazone bond formation, while the sulfhydryl chemistry utilizes nanocrystals displaying surface activated maleimide groups. Both reactive chemistries are rapidly implemented, yielding purified nanocrystal—protein bioconjugates in as little as 3 h. Following initial characterization of the nanocrystal materials, the wide applicability and strong multiplexing potential of these chemistries are demonstrated in an array of applications including immunoassays, immunolabeling in both cellular and tissue samples, *in vivo* cellular uptake, and flow cytometry. Side-by-side comparison of the immunolabeled cells suggested a functional equivalence between results generated with the amine and thiol-labeled antibody—nanocrystal bioconjugates in that format. Three-color labeling was achieved in the cellular uptake format, with no significant toxicity observed while simultaneous five-color labeling of different epitopes was demonstrated for the immunolabeled tissue sample. Novel labeling applications are also facilitated by these chemistries, as highlighted by the ability to directly label cellular membranes in adherent cell cultures with the thiol-reactive chemistry.

KEYWORDS: nanocrystal · semiconductor · quantum dot · bioconjugation · chemoselective · probe · cellular imaging · multiplexing

Since the seminal introduction of water-soluble luminescent semiconductor nanocrystals (NCs) or quantum dots as fluorescent probes more than a decade ago,[1,2] interest in utilizing these unique optical nanomaterials in diverse biological applications continues to grow almost unabated.[3,4] Demonstrated biological applications to date include cellular labeling, *in vivo* imaging, sentinel lymph node mapping, single molecule tracking, myriad immunochemistries, Förster resonance energy transfer (FRET) sensing, photodynamic therapy, nanomedicine research, and multimodal cancer targeting platforms, to name but a paltry few.[3,5−13] The principal impediment to further biological utility continues to be the limited chemistries for attaching biologicals such as antibodies and other proteins to the NCs in a facile, widely applicable manner that still yields controlled, functional nanoparticle bioconjugates capable of cellular uptake and other labeling utility. NC surfaces must be tailored and optimized for use in a specific application and indeed substantial resources continue to be devoted toward this.[14−17] Available NC bioconjugation chemistries generally target the ubiquitous amine and carboxyl functional groups present on proteins or the less prevalent thiols that are sometimes recombinantly introduced for site-specific labeling.[18]

Carbodiimide (EDC)-based chemistry is the most common strategy used to join carboxylated NCs to protein amines *via* amide bond formation. As currently applied, this approach is plagued by several unresolved issues, including EDC's rapid hydrolysis in aqueous environments,[18] the need for many 1000-fold excesses of reactive reagent, and susceptibility to cross-linking, all of which often results in heterogeneous conjugate architecture and mixed avidity. In practice, these issues usually require multiple trial and error attempts prior to achieving a viable conjugate. As NCs are commonly made water-soluble with thiolated bifunctional surface ligands,[19] thiol-coupling chemistry is also complicated. Proteins displaying accessible thiols can be directly coordinated to the NC surface, although the

* Address correspondence to travis.jennings@ebioscience.com, igor.medintz@nrl.navy.mil.

Received for review March 20, 2011 and accepted June 8, 2011.

Published online June 21, 2011
10.1021/nn201050g

dynamic on−off rate of this attachment usually yields conjugates with limited stability and activity.[19,20] Derivative conjugation attempts have explored incorporating heterobifunctional linkers to target the (bio)thiols, however, these add more steps and complexity to the chemistry while lowering overall yield.[21] Although highly effective, alternate conjugation strategies incorporating chemical or affinity handles such as polyhistidine tags for self-assembly, arsenic-vicinal tetracysteine motifs, or "click-chemistries", like tetrazine-norbornene cycloaddition, require extensive protein and NC engineering.[14,15,22] Biotin−avidin chemistry is also a common approach to QD bioconjugation, however, this still requires the requisite labeling of both QD and target biomolecule and usually yields heterogeneous structures, while multibiotinylated molecules frequently cross-link and precipitate the QDs.[18−20] Improved chemistries targeting the same amine/thiol functionalities still remain highly desirable. Here we introduce two new reactive, orthogonal NC bioconjugation chemistries that overcome many of the aforementioned issues. Both chemistries are rapidly implemented, yielding purified NC−protein conjugates in as little as 3 h. We demonstrate their wide applicability and strong multiplexing potential in an array of applications including immunoassays, flow cytometry, immunocytochemistry, immunohistochemistry, and *in vivo* cellular uptake/labeling.

RESULTS

Nanocrystals. CdSe/ZnS core/shell eFluor (eF) NCs with photoluminescence (PL) maxima centered around 525, 565, 605, 625, and 650 nm (Figure 1A,B) were synthesized using standard high temperature reactions of organometallic precursors in hot coordinating solvents.[23] NC samples are designated by their discrete PL maxima (*i.e.*, eF605 NC refers to a 605 nm emitting nanocrystal; materials lacking the NC designation are other types of fluorophores). NC photophysical properties including the extinction coefficients, PL emission wavelength, full width at half-maximum (fwhm), and quantum yield (QY) in aqueous solution are presented in Table 1. NCs were stabilized in water using a DSPE-PEG lipid (1,2-distearoyl-*sn*-glycero-3-phosphoethanolamine-*N*-[carboxy(polyethylene glycol)-2000], chemical structure provided in Supporting Information) as previously described.[24] NC surfaces were further modified with 4-formylbenzamide (4FB) or a reactive maleimide using proprietary techniques at eBioscience (San Diego, CA). After maleimido-activation, the NCs were lyophilized and stored under vacuum at 4 °C until use. Both types of NCs prepared in this manner remain stable for at least 1 year.

Amine-Reactive Chemistry. The amine targeting conjugation utilizes a bioorthogonal ligation reaction to link biomolecular amines to preactivated NCs. As shown in Figure 1C, the primary amine(s) on the target biomolecule are first modified with a heterobifunctional *N*-hydroxysuccinimidyl ester 6-hydrazinonicotinamide (NHS-HyNic, SoluLink). Excess HyNic is removed with a desalting spin column postmodification, as described in the Materials and Methods. The HyNic-modified biomolecule is then added to a solution of 4FB-modified NCs along with aniline as a catalyst, and the conjugation reaction proceeds for 2 h forming a bis-aryl hydrazone bond between the 4FB and HyNic moieties. NC conjugates are then transferred to a 100 kDa centrifuge filter (Millipore) diluted with 100 mM borate buffer, pH 8.4, and buffer exchanged at least three times to remove unreacted antibodies or proteins and catalyst. Lastly, purified conjugates are microcentrifuged briefly at 1000 × *g* for 5 min to remove any undissolved solids and cross-linked materials.

Aniline-catalyzed hydrazone ligation chemistry originates from the Dawson Laboratory and is characterized by enhanced bioconjugation rates of 10^1-10^3 M^{-1} s^{-1} in mild, aqueous conditions (slightly acidic to neutral pH).[25−27] This stoichiometric chemistry has been shown to go to completion in under 30 min using 100 mM aniline catalyst with 10 μM of reactants and forms stable conjugates. As the hydrazine and aldehyde reactants are orthogonal to almost all biological functionalities, they do not alter the subsequent structure or capabilities of other groups already present in the NC bioconjugate.

Sulfhydryl-Reactive Chemistry. The sulfhydryl chemistry employs reactive maleimide functionalities introduced onto the NC surface to target free biomolecular thiols, including those in the hinge region of antibodies, Figure 1D.[18] Prior to conjugation, the NCs are warmed to room temperature and vented to atmospheric pressure. Lyophilized NCs are reconstituted by adding 100 μL of phosphate-buffered saline, pH 7.4 (PBS), and swirled briefly in a 60 °C water bath. After the solution becomes optically clear, 200 μg antibody equivalent is pipetted directly in with the reactive NC, which contains a proprietary reducing agent, and is allowed to react for 2 h. The reaction is then quenched by adding 1 μL of 2-mercaptoethanol (2-Me) for an additional 10 min. The NC conjugates are then transferred to a 100 kDa centrifuge filter (Millipore), diluted with 100 mM borate buffer, pH 8.4, and buffer exchanged at least three times to remove unreacted antibody and 2-Me. Lastly, the purified conjugates are microcentrifuged briefly at 1000 × *g* for 5 min to remove any undissolved materials and cross-linked NCs. Detailed descriptions of the NC labeling and the assay procedures can be found in the Materials and Methods.

Nanocrystal Characterization. Prior to applying the NC conjugates, we first examined their relevant optical and physical characteristics. Figure 1A,B and Table 1 confirm that NC emission and fwhm are indeed narrow

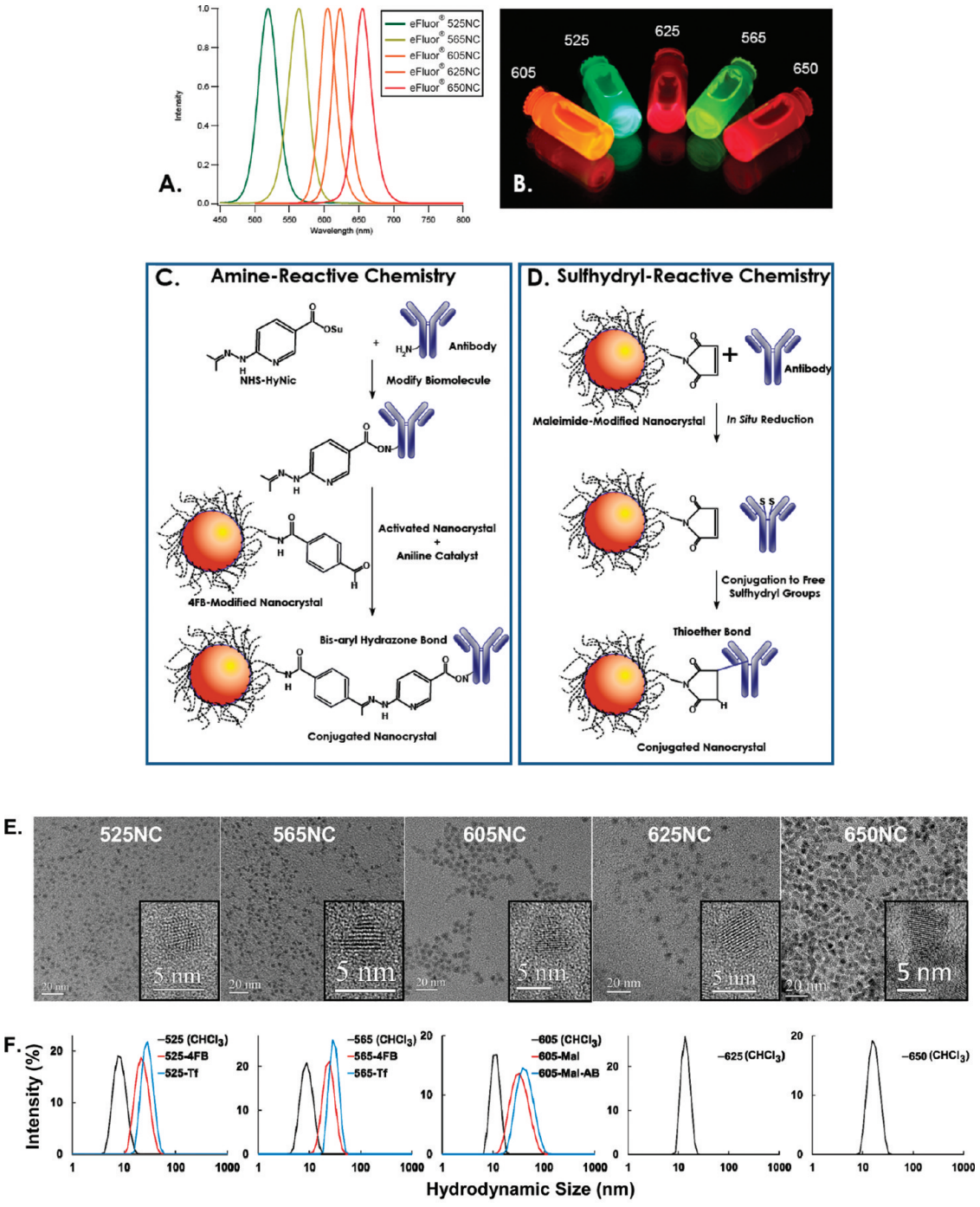

Figure 1. Nanocrystal materials and amine-reactive and sulfhydryl-reactive conjugation chemistry. (A) Photoluminescence spectra for eFluor Nanocrystals and (B) visible image of NCs in solution under short-wave UV excitation. (C) Schematic of the amine-reactive chemistry in which free primary amine(s) on a biomolecule is first modified with succinimidyl 6-hydrazinonicotinate acetone hydrazone (S-HyNic). The resulting hydrazine group on the biomolecule is then specific for a premodified 4-formylbenzamide (4FB) NC and the conjugation reaction take place rapidly in the presence of an aniline catalyst (2 h). (D) Schematic of the sulfhydryl-reactive chemistry, which consists of a maleimide-functionalized NC and an *in situ* reducing agent. Biomolecules containing either disulfide bonds or available sulfhydryl groups are directly reduced in solution with reactive NCs for immediate conjugation. Note: not to scale. (E) HR-TEM of as synthesized eF525, eF565, eF605, eF625, and eF650 NC samples. The inset lower right shows a higher power magnification micrograph of an individual NC. (F) Hydrodynamic size distribution of selected native NC samples in $CHCl_3$, along with 4FB, maleimide, and protein-modified samples. Corresponding H_D values are presented in Table 2 and the Supporting Information.

(27−35 nm), which allows them to be relatively well-separated spectrally from each other, except for the eF605 and eF625 pair. Moreover, encapsulation within the DSPE-PEG lipid maintains high QYs that are in the 60−70% range. The NC core/shell structures were visualized with high resolution-transmission electron

TABLE 1. Select Photophysical Properties of the Nanocrystals Utilized

NC sample	emission wavelength (nm)	fwhm (nm)	extinction coefficient[a] (M^{-1} cm^{-1})	quantum yield[b] (%)
eFluor 525NC	527	35	5.57×10^4	63
eFluor 565NC	566	30	1.12×10^5	60
eFluor 605NC	608	27	2.85×10^5	64
eFluor 625NC	628	29	5.21×10^5	70
eFluor 650NC	651	27	1.12×10^6	68

[a] Extinction coefficient at the first exciton absorption peak for each nanocrystal. [b] Quantum yields measured relative to either FITC in basic ethanol (eF525NC) or R6G in ethanol.

TABLE 2. Select Physical Characteristics of the Nanocrystals Utilized

sample description		HR-TEM[a] diameter (nm)	Z-potential (mV) in buffer[b]	DLS hydrodynamic diameter H_D (% intensity)[c]
NC (as-synthesized)	eF-525NC ($CHCl_3$)	4.3 ± 0.3		8.4 ± 2.3
	eF-565NC ($CHCl_3$)	4.8 ± 0.3		9.0 ± 2.3
	eF-605NC ($CHCl_3$)	6.1 ± 0.4		11.2 ± 2.2
	eF-625NC ($CHCl_3$)	7.1 ± 0.5		14.0 ± 2.7
	eF-650NC ($CHCl_3$)	8.7 ± 0.5		17.0 ± 4.4
NC-4FB	eF-525NC-4FB		−2.7 ± 1.1	23.0 ± 6.7
	eF-565NC-4FB		−3.8 ± 0.6	24.2 ± 6.3
	eF-605NC-4FB		−3.5 ± 1.4	26.9 ± 9.0
NC-maleimide	eF-525NC-maleimide		−4.6 ± 1.0	26.3 ± 6.9
	eF-565NC-maleimide		−6.0 ± 0.7	30.7 ± 8.0
	eF-605NC-maleimide		−5.0 ± 0.1	35.0 ± 13.9
NC-protein	eF-525NC-Tf		−2.1 ± 0.8	28.9 ± 7.1
	eF-565NC-Tf		−3.3 ± 0.7	30.5 ± 6.2
	eF-605NC-mal-antibody		−8.1 ± 0.5	44.1 ± 16.7

[a] Estimated from analysis of at least 100 NC structures per sample. [b] Measured in borate buffer as supplied (0.1 M sodium tetraborate, 0.3 M NaCl, ~0.01% sodium azide, pH 8.3). [c] Due to the diverse ways to represent data, the hydrodynamic diameters characterized by different profiles are shown here for comparison. Intensity profile is used for the present discussion. Corresponding volume and number profiles are provided in the Supporting Information. Tf = transferrin.

microscopy (HR-TEM), while the hydrodynamic diameter (H_D) of native "as synthesized" NCs, along with representative lipid-coated and protein-modified NCs, were measured using dynamic light scattering (DLS). A detailed description of the analytical protocol is provided in the Supporting Information. As presented in Table 2 and Figure 1E,F, the NC core/shell "hard" diameter increases in size from 4.3 to 8.7 nm, as expected with the red-shift in PL maxima. Observed NC shapes are not completely spherical and tetrahedron-like structures are visualized for the larger-sized NC samples. Crystalline lattice structures are clearly visible for each NC in the high-resolution micrograph provided with each sample, see Figure 1E inset. The H_D of the unmodified NC materials was found to be consistently almost twice the hard diameter (8.4−17 nm in intensity profiles). The differences in sizes between H_D and hard core/shell size measured in all samples arises from the hydrodynamic interactions of the native coordinating ligand, mostly trioctyl phosphine oxide (TOPO), on the NC surface in toluene.[23]

A representative set of eF525, eF565, and eF605 NC samples displaying either the 4-FB amine-chemistry activation, reactive-maleimide, or conjugated proteins were also compared using DLS analysis (Table 2 and Figure 1F). The H_D of the 4FB and maleimido-activated NCs are comparable within the error values of each analysis; the slight differences in size are attributed to subtle contributions from the 4-FB or slightly larger maleimido-reactive group. These sizes, however, are significantly larger than that of the native NCs in organic solvents. This is directly attributable to the bulk size of the DSPE-PEG lipid ligand, which interdigitates with the NC's native surface, while the PEG moiety mediates solubility (see Supporting Information, structure 1). Although displaying a high degree of flexibility, the ~45 ethylene oxide repeat units within each ligand's distal PEG unit will increase the H_D considerably, and the increases in size observed are slightly larger than a geometrical approximation of the ligand in a fully extended confirmation. eF525 and eF565 NC-4FB conjugated to human transferrin (~80 kD) and eF605-NC-maleimide conjugated to an antibody (~150 kD) were analyzed with DLS and also displayed the requisite increases in H_D, confirming conjugation. In addition, conjugating the larger antibody to the eF605 NC resulted in the largest increase in H_D. We do recognize that the hydrodynamic volume of a colloidal NC is far more complex than the simple approximations described here and is controlled by

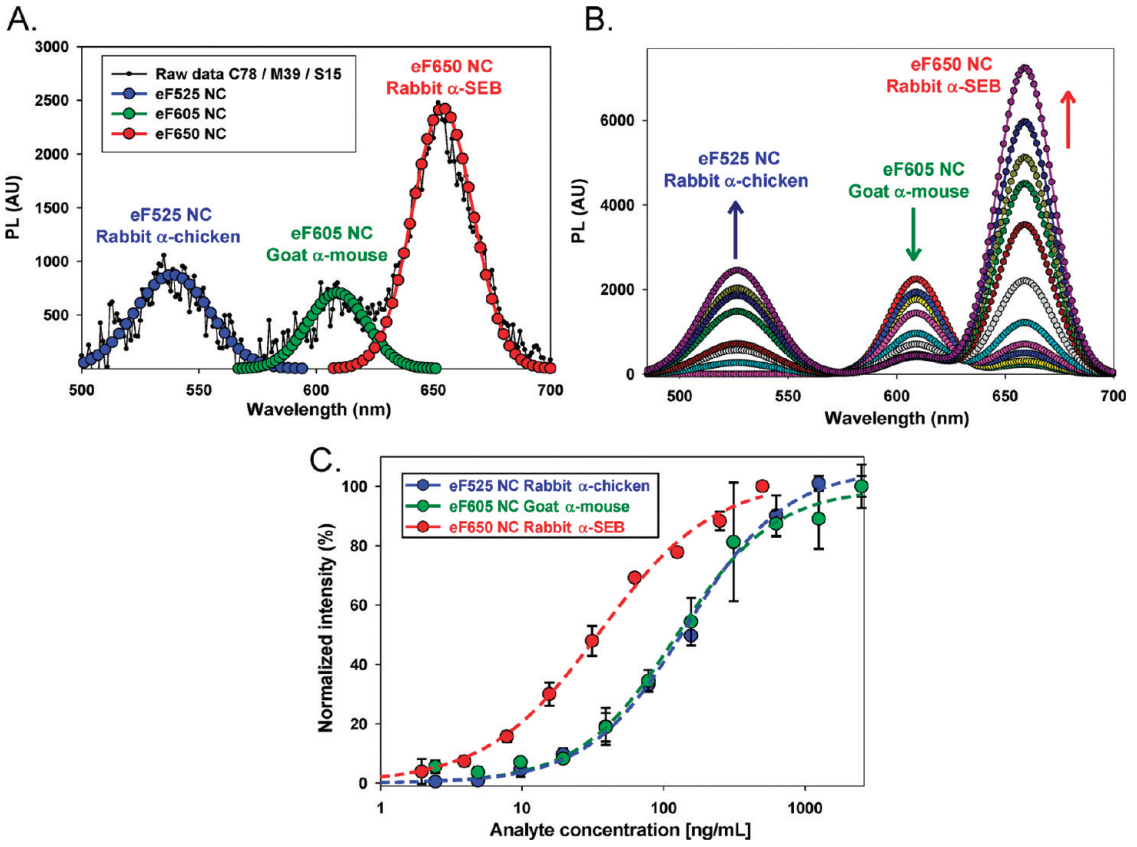

Figure 2. Simultaneous triplex immunoassay. (A) Fluorescence intensity wavelength scan of a microtiter well exposed to chicken IgG (78 ng/mL), mouse IgG (39 ng/mL), and SEB (15 ng/mL), followed by the triplex NC-antibody tracers. The spectra shown include the raw data taken using the Tecan plate reader and the deconvoluted fitted data for each of the NC-antibody conjugates. (B) Fitted data of the triplex immunoassay fluorescence intensity wavelength scans for all 12 wells exposed to mixed concentrations of chicken IgG (C: 0−2500 ng/mL), mouse IgG (M: 0−2500 ng/mL), and SEB (S: 0−500 ng/mL). Increments of antigen concentrations are in 50% dilutions from the maximum shown for each. (C) Normalized intensity data, taken from the fluorescence plate reader, for each of the analytes studied in the triplex immunoassay. Intensities normalized to the highest concentration measured. LODs were 10 ng/mL chicken IgG, 5 ng/mL mouse IgG, and 2 ng/mL SEB.

not only the size and chemical nature of the surface coatings but also by the NC size itself along with the nature of the solvation layer, relative charges and solvent. The zeta potential (ζ) of these same materials in borate-based purification buffer (see Materials and Methods) was found to be consistently slightly negative (<-10 mV), reflecting the basic charge of the media. Values in buffer are of a smaller magnitude than measured in water (Supporting Information) due to the higher ionic strength that can screen the NC surface charge and decrease apparent ζ values. Having verified the high QY and small relative size of the NC materials, we next applied them to select bioassays.

Immunoassays. We began evaluating the NC-conjugation chemistry utility in immunoassays. In all their various formats, these continue to be one of the mainstay biotechnologies used in diverse applications ranging from monitoring water and food supplies to diagnosing cancer.[28−30] In many circumstances, multiplexing (simultaneously probing mixed samples) is highly desirable to increase throughput, reduce cost/time/reagents, increase data generation, and simplify formats.[31] Beyond cross-reactivity, the major impediment to multiplexing in fluorescent immunoassays, however, continues to be the photophysical properties and emission overlap of the commonly used organic dye labels that preclude use of simplified optical setups.[32,33] A triplex sandwich immunoassay was conducted to evaluate the performance of NC-antibody probes assembled using maleimide chemistry. The target analytes utilized here include two closely-related immunoglobulins (IgGs) to monitor for potential cross-reactivity and one unrelated protein toxin.

eF525, eF605, and eF650-maleimide NCs were conjugated to rabbit anti-chicken IgG, goat anti-mouse IgG, and rabbit anti-staphylococcal enterotoxin B (SEB), respectively. SEB is a 240 residue protein (~28 kD) produced by *Staphylococcus aureus* bacterium and is one of the toxins commonly associated with food poisoning. The MW of the IgGs is estimated to be ~150 kD. Microtiter well plates were functionalized with capture antibodies, blocked, and exposed to different concentrations of each IgG and SEB analyte, as described in the Materials and Methods. In the target samples, chicken IgG and SEB concentrations were serially increased from 0 to 2500 ng/mL and 0 to

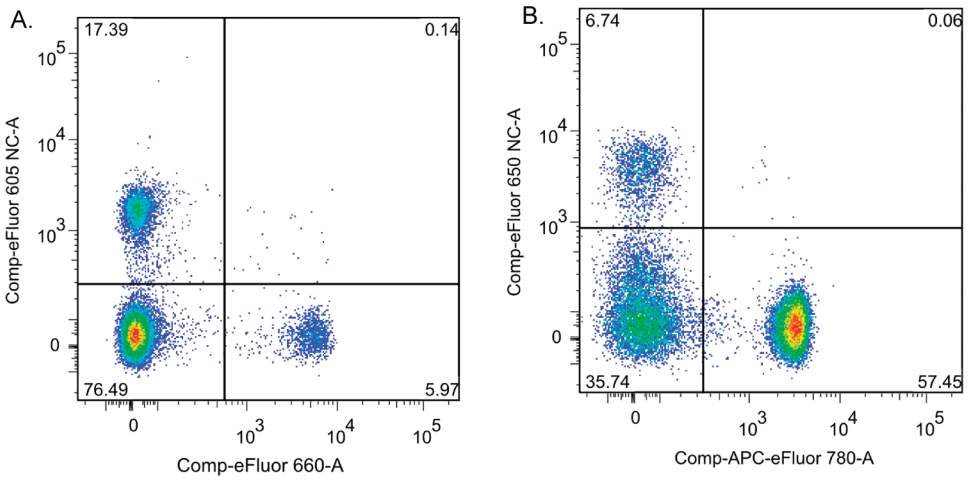

Figure 3. Flow cytometry analysis. Two-color flow cytometry data using antibodies conjugated to NCs in combination with standard organic dye or fluorescent protein–antibody conjugates. (A) Staining of mouse splenocytes with anti-mouse CD4 antibody conjugated to eF605 NCs using amine-reactive chemistry (*y*-axis) and eF660-conjugated anti-mouse CD8α (*x*-axis). The negative cell population (lower left) is primarily B cells and natural killer cells. CD4+ cells show increased fluorescence intensity in the eF605 NC channel along the *y*-axis (upper left), and eF660-anti-mouse CD8α only positive cells (lower right) show increased intensity along the *x*-axis. (B) Staining of normal human peripheral blood cells displays a similar pattern, with eF650 NC-anti-human CD8α conjugated using sulfhydryl-based chemistry. CD8α+ cells stained with eF650 NC-anti-human CD8α (upper left) are discretely resolved from CD4+ cells costained with APC-eF780-anti-CD4 (lower right). The values in each corner reflect the percentage of the total number of cells present in that quadrant. eF660 and eF780 are organic dye derivatives. See Materials and Methods for experimental details.

500 ng/mL, respectively, while mouse IgG was concomitantly decreased from 2500 to 0 ng/mL. A mixed solution of the NC tracers at preoptimized dilutions was used to probe the samples for 1 h, followed by fluorescence scanning. In Figure 2A, a representative example of a composite trace and the background-subtracted deconvoluted, fitted spectra gathered from a sample exposed to one of the lower analyte concentrations are presented. Samples were deconvoluted using a triple Gaussian function in a manner similar to that previously described.[34,35] Figure 2B shows the full series of deconvoluted, fitted spectra in a superimposed plot (raw data shown in Supporting Information). Figure 2C compares the normalized intensity data versus concentration for each analyte in the triplex mixture. This data also provided estimates of the limit of detection (LOD, corresponding to the analyte concentration at which signal was greater than the blank plus 3 times its standard deviation) for this triplex format of 10 ng/mL chicken IgG, 5 ng/mL mouse IgG, and 2 ng/mL SEB. The latter SEB LOD is significantly improved from the 30 ng/mL reported in a previous four-color NC immunoassay.[34] Although quite powerful, the previous protocol required attaching antibodies to the NCs with adaptor proteins *via* a multistep procedure that also necessitated affinity-column purification. Here, changes in analyte concentrations relative to each other in the triplex are clearly visualized across the entire concentration range, even prior to deconvolution. This is greatly facilitated by the excellent spectral separation between NC peak emission wavelengths, which ranged from 45 nm up to 80 nm (distance between the PL maxima), depending on color, combined with their narrow fwhm values, all of which minimize spectral cross-talk and simplify the Gaussian fitting and deconvolution during subsequent analysis. More importantly, all data were collected with a single 400 nm excitation wavelength and one spectral emission window from the same assay plate (see Materials and Methods). Although only an initial test, the NC-antibody constructs are able to differentiate among related IgG proteins and between small and large proteins even when all are present in the same assay. Clearly far denser multiplex immunoassays in many different formats (*i.e.*, capture, direct, displacement, *etc.*) are possible beyond the triplex sandwich assay demonstrated here.

Multicolor Flow Cytometry. In contrast to the immobilized microtiter-well assays described above, NC-antibody conjugates were next applied in four-color flow cytometry to demonstrate their utility in discriminating large cellular targets. Figure 3A shows a representative two-color flow cytometric dot plot obtained from the staining of mouse (Balb/c) splenocytes with anti-mouse CD4 antibody conjugated to amine-reactive eF605 NCs in combination with anti-mouse CD8α antibody conjugated to eF660 organic dye (see Materials and Methods for additional data). Cell surface receptors such as CD4 and CD8a are displayed differentially on immune cells such as T lymphocytes and their expression is frequently used to identify and correlate helper and cytotoxic T cell populations, respectively. Results clearly demonstrate that the eF605 NC-conjugated CD4 antibody can resolve the helper T cells as a discrete population (Figure 3A, upper left) away from the cytotoxic T cells (lower right). Moreover, cells

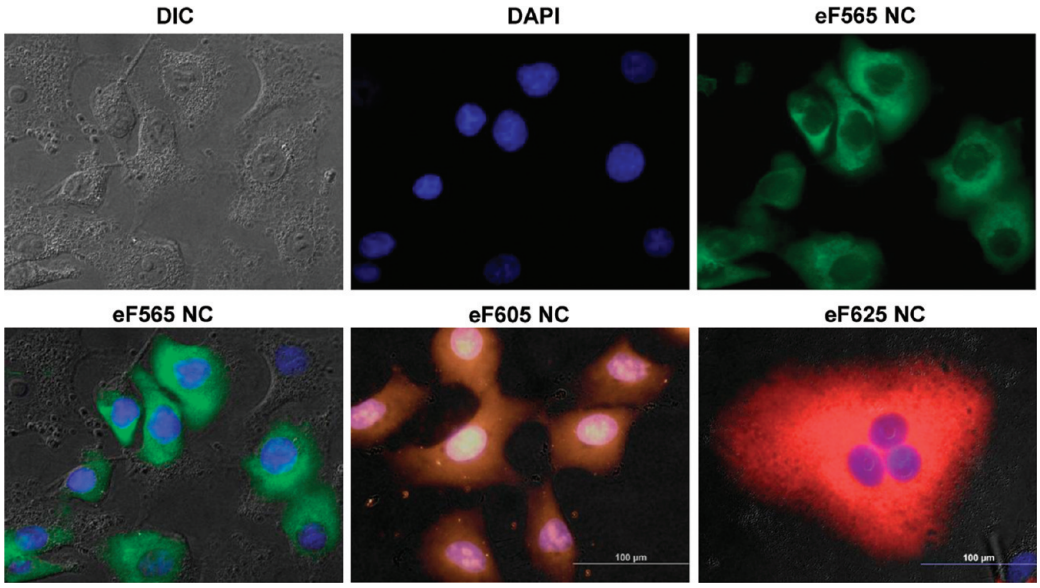

Figure 4. Labeling of cellular membranes. A549 cellular membranes directly labeled with 125 nM solutions of eF565 NC, eF605 NC, and eF625 NC using sulfhydryl-reactive chemistry. Top panel shows the separate DIC (differential interference contrast), DAPI (nuclei), and eF565 NC emission for the eF565 NC-labeled cells. Composite fluorescent images for each NC in the bottom panel were assembled using separate DIC, NC, and DAPI fluorescence. False color (orange) is used for the eF605 NC fluorescence. A multinucleated cell is highlighted and labeled with eF625 NC on the bottom right. Imaging is described in the Materials and Methods.

that do not express the CD4 or CD8 antigen in the spleen, such as B cells and natural killer cells, do not exhibit any staining with either antibody (lower left). Figure 3B presents a similar two-color dot plot obtained by staining normal human peripheral blood cells with sulfhydryl-reactive eF650 NC-conjugated anti-human CD8α antibody and anti-human CD4 conjugated to an APC-eF780 tandem organic fluorophore. APC-eF780 is a tandem FRET construct consisting of the 104 kD allophycocyanin (APC) fluorescent protein complex from red algae functioning as a donor to a 780 nm emitting organic dye, demonstrating the utility of multiplexing with NCs in systems where other complex fluorophore arrangements are also present. As expected, data demonstrates distinct staining of the CD8α+ cytotoxic (upper left) and CD4+ helper T cells (lower right), enabling discrimination of these populations away from other cell types present in human peripheral blood, including B cells, natural killer cells, and monocytes.

In both assays, staining with the NC-conjugated antibody exhibited low background, distinct separation from the negative population and low nonspecific staining of other cell populations. These data were as expected and comparable to controls utilizing standard dye-labeled antibodies collected in the same format (Supporting Information, Figure 2), showing that NC-antibody conjugates do not interfere and that they may be used to augment assays incorporating standard antibody−dye conjugates while still producing the expected results. This potentially allows the flexibility of adding custom NC−antibody conjugates in combination with existing panels of organic dye-labeled antibody conjugates. Similar to the immunoassays described above, incorporating NCs can also enable dense multiplexing in flow cytometry, while the ability to excite multiple NC colors with one excitation laser greatly simplifies instrumental requirements.[36]

Direct Labeling of Cellular Membranes. When visualizing cells and subcellular organelles such as nuclei, especially following fixation, it is quite useful to selectively stain the membrane for fluorescent contrast. The sulfhydryl-reactive chemistry was utilized to directly accomplish this in a rapid 3-step manner consisting of incubation and two washes. Human adenocarcinoma alveolar basal epithelial A549 cells were seeded in chambered coverwell slides precoated with fibronectin. As described in the Materials and Methods, following overnight growth, cellular monolayers were fixed with paraformaldehyde, washed, and blocked with PBS containing bovine serum albumin. Select chambers were then exposed to solutions of reconstituted eF565, eF605, or eF625-maleimide NCs directly for 1 h. Cells were then washed twice with PBS, followed by counterstaining of the nuclei with DAPI. As can be seen in Figure 4, where each image highlights a different NC color used, cellular membranes are almost exclusively labeled using this strategy. Importantly, no background labeling of the fibronectin-coated coverslip was seen, even at the highest NC concentrations used (250 nM). We noted labeling of >85% of the cells present when using 125 nM NC solutions, which could be increased to ~100% by using the higher 250 nM NC

concentrations. Further exposure of these labeled cells to DAPI during the counterstaining did not appear to affect NC fluorescence, suggesting that the NCs are well protected and relatively inert to their environment following labeling. Similar staining appeared to be equally efficient in other cell types (data not shown). We surmise that this chemistry specifically targets free-thiols or reduced protein disulfides present on the extracellular membrane and that small differences in labeling efficiency may arise from heterogeneous expression of thiolated-cell surface proteins. The unique options of (1) specifically labeling cellular membranes in a particular sample, with the option of (2) selecting a desired PL color, while also (3) not requiring labeled-antibodies directed against extracellular components (*i.e.*, integrins) as recognition mediators can greatly simplify multicolor fluorescent staining experiments.

Multicolor Immunocytochemistry and Immunohistochemistry. To further confirm that no significant differences would arise from the joint use of either amine or sulfhydryl-labeling chemistry, we labeled the same set of two antibodies targeting acidic cytokeratin and α-tubulin with each chemistry and then applied these along with an organic-dye labeled antibody targeting Ki-67 protein within a multicolor coimmunolabeling protocol (see Materials and Methods). Cytokeratins are a large family of filament proteins that are developmentally regulated and comprise a significant portion of the cytoskeleton in epithelial cells. As many tumors also express different cytokeratins, visualizing and classifying them in specimens can help identify their origin.[37,38] Tubulin is the primary component of microtubules in the cytoskeleton and is structurally rearranged during lifecycle processes such as mitosis. Ki-67 protein is used as a nuclear marker of proliferating cells, where it is actively visualized during all phases associated with the cell cycle. Within a particular tumor sample or biopsy, relative Ki-67 expression levels can be used to determine the fraction of proliferating cells.

As presented in Figure 5A, MCF-7 epithelial breast cancer cells were cultured, fixed, blocked and then simultaneously immunostained with the three dye/NC-labeled antibodies overnight. Anti-cytokeratin targeting the five acidic cytokeratins in the 40−56.5 kDa range was conjugated to eF605 NCs. Mouse monoclonal anti-α-tubulin, which recognizes residues 426−450 of the tubulin protein, were attached to eF650 NCs and mouse monoclonal anti-Ki-67, which binds the 345 and 395 kDa Ki-67 protein isoforms, was labeled with Alexa-Fluor dye. The figure shows a side-by-side comparison of representative micrographs where PL was collected from each NC/fluorophore-antibody color along with merged fluorescent images and a higher power magnification (40×) micrograph of individual cells. Clearly, the resulting pattern of staining and fluorescence are almost identical, and no remarkable differences were observed between each set of images. Targeting the ubiquitous amines or far fewer thiols on these antibodies for NC-modification did not alter the overall activity of the antibodies. The only difference is a slight variation in the concentration of each NC-antibody conjugate applied during staining, see legend of Figure 5. This shows that NC conjugates prepared using both chemistries can effectively colabel different components of the same subcellular structures in conjunction with traditional dye-labeled antibodies. It is important to note that this chemical flexibility will be particularly useful in cases where the amines on antibody binding sites may be preferentially modified or reduction of the thiol-hinge region significantly alters binding site structure; either of these may result in a loss of activity. It is also possible that the 3-dimensional size and bulk of the reactive NCs precludes chemical access to amines located deep within the antibody structure and thus favor a superficial surface attachment.

Confident in the ability to mix and match NC−antibody conjugates created with both chemistries in multiplex formats, we next performed a five-color immunohistochemical labeling in a fixed tissue sample (Figure 5B). Mouse spleen was utilized as the test sample and probed with antibodies that targeted different components of the immune system including B and T cells, leukocytes, and the macrophages present in this tissue milieu. B cells were labeled with eF525 NCs functionalized with anti-B220 antibody, which binds a type C protein tyrosine phosphatase receptor, also known as CD45 antigen. This protein is expressed as a heavily glycosylated 220 kD variant on the follicles of B cells. Leukocytes and endothelial cells were visualized with anti-PECAM-1 (platelet endothelial cell adhesion molecule) functionalized with eF565 NCs. PECAM-1 or CD31 is an ∼135 kDa surface protein expressed at low levels on all leukocytes and functions in cell−cell adhesion and signal transduction. Anti-CD11c was attached to eF650 NCs to target integrin αX expressed by some activated T cells and which is also found on dendritic cells in T-dependent areas of the mouse spleen. eF605 NCs were coupled to anti-CD11b, which recognizes the ∼170 kDa integrin αM found on macrophages. Lastly, eF625 NCs were labeled with anti-CD4, which targets thymocytes, as described above. eF525 and 565 NC labeling utilized amine chemistry, while eF605, 625, and 650 NCs were functionalized using the sulfhydryl chemistry. All antibodies used were monoclonal rat or hamster anti-mouse isotypes to optimize specificity. Details of the labeling, antibody incubation protocol, and imaging can be found in the Materials and Methods. It should be noted that, while the matching of a particular chemistry with an antibody was random, the NC color choices were assigned based on expected expression levels of the antigen. This provided a matching of the smaller NCs displaying a lower extinction coefficient (see Table 1)

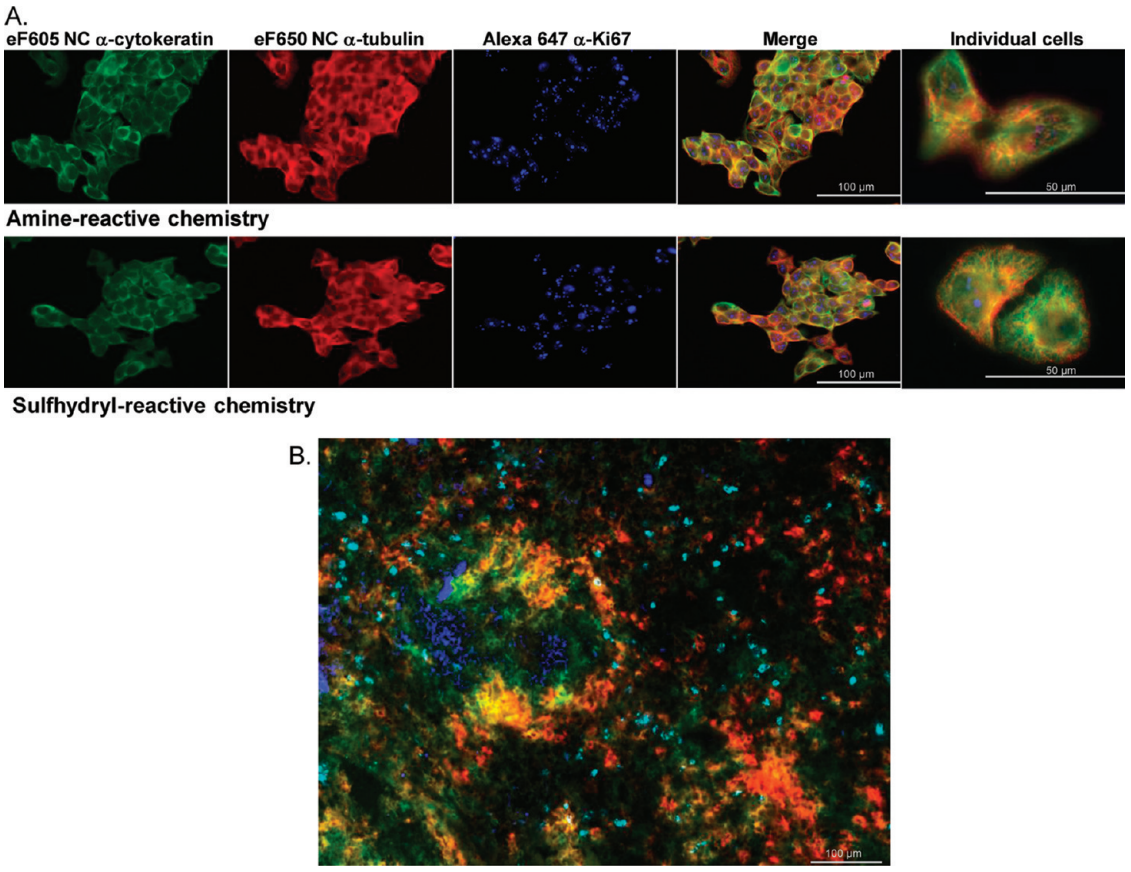

Figure 5. Multicolor immunocytochemical labeling with amine- and sulfhydryl-reactive NCs. (A) For each panel, fluorescent micrographs show the eF605 NC emission (false-colored green), eF650 NC emission (false-color red), AlexaFluor 647 emission (false-color blue), and the merged fluorescence. Higher magnification images of individual cells labeled using each chemistry are also shown. Top panel: Following growth and fixation, MCF-7 epithelial breast cancer cells were probed with 20 nM eF605 NC-anti-cytokeratin and 0.5 nM 650 NC-anti-tubulin conjugates along with 5 μg/mL Alexa 647-labeled anti-Ki-67. The NC−antibody conjugates for this panel were prepared with the amine-reactive chemistry. Bottom panel: Cells prepared in the same manner probed with 40 nM eF605 NC−anti-cytokeratin and 1 nM eF650 NC−anti-tubulin conjugates and with 5 μg/mL Alexa 647-labeled anti-Ki-67. NC−antibody conjugates for this panel were prepared with the sulfhydryl-reactive chemistry. (B) Five-color immunohistochemical labeling of a mouse spleen tissue section simultaneously stained with amine- and sulfhydryl-reactive antibody-bound NCs. Merged fluorescence-false color image of the five separate NC−antibody conjugates and analyzed with a multispectral imager. Conjugate/color-scheme is as follows: eF525-B220/blue, eF565-PECAM-1/yellow, eF605-CD11b/aqua, eF625-CD4/green, and eF650-CD11c/red. The eF525 and eF565 NC-labeling utilized amine chemistry, while the eF605, eF625, and eF650 NCs were functionalized using sulfhydryl chemistry.

with the higher expressing antigen and *vice versa*, which cumulatively allowed for a better normalization of probe intensity and the required exposure times for all probes in a multiplexed system.

A representative merged fluorescent micrograph collected using multispectral imaging and pseudocoloring is shown in Figure 5B where eF525 NC-B220 appears in blue, eF565 NC-PECAM-1 in yellow, eF605 NC-CD11b in aqua, eF625 NC-CD4 in green, and eF650 NC-CD11c in red. Individual macrophages are clearly visible arrayed around the periphery by their punctate aqua staining. A grouping of B-cells (blue) appears to the left of center and is closely associated with both leukocytes and endothelial cells (yellow). CD4+ thymocytes (green) are found adjacent and interspersed into the B-cell center (blue). Activated T-cells and dendritic cells (red) surround the B-cell and T-cell areas and are found as individual cells throughout the tissue. Dendritic cells are highly motile and a concentration of these cells is seen in the lower right field of view, which may represent the site from which the dendritic cells are migrating into the spleen tissue. The distribution of NC-labeled cells is typical of staining patterns in the spleen when using single-color immunohistochemistry to localize different cell types, showing that the specificity of individual NC-labeled antibodies is maintained even in multiplexed conditions. Importantly, the multiplexing capabilities highlighted in this image reflect how NCs can help contribute to understanding the complex interplay of these different cells by allowing visualization of their specific localization within tissues in a facile manner.

NC Uptake in Live Cells. To evaluate whether NC−protein conjugates could undergo facilitated uptake to cultured cells *in vivo* in a controlled manner, we selectively labeled NCs with the iron transport protein

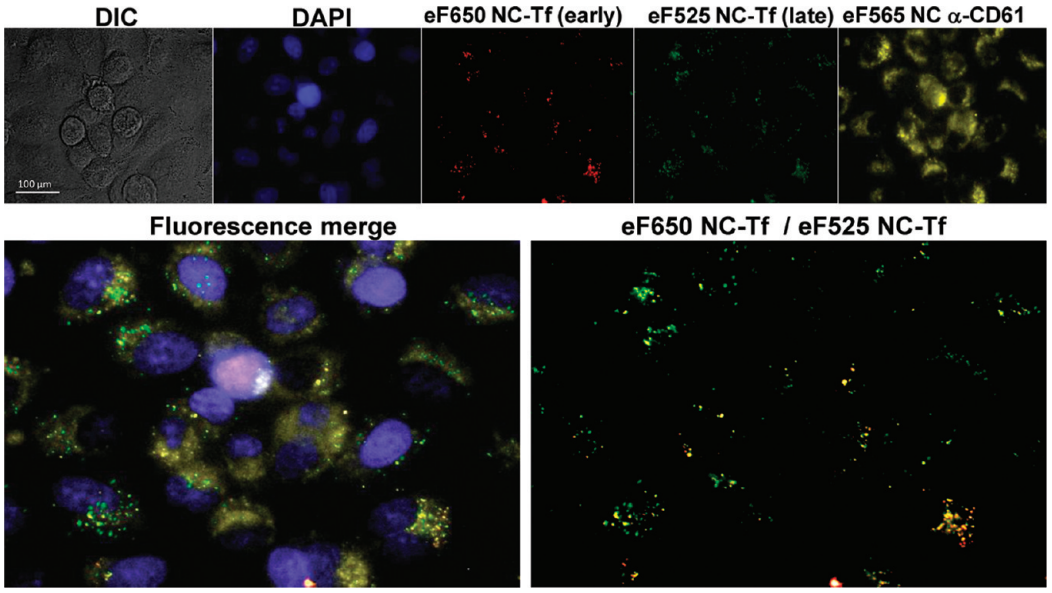

Figure 6. Multicolor labeling of early and late endosomes and the cellular membrane (integrins). Live A549 cells were sequentially labeled with eF650 and eF525 nanocrystals conjugated to transferrin (Tf) followed by fixation and labeling of cell membrane integrins with eF565 NC conjugated to anti-CD61 antibody. Top panel: Shown are DIC, DAPI (nuclei), eF650 NC-Tf (early endosomes), eF525 NC-Tf (late endosomes), and eF565 NC-anti-CD61 (membrane integrins). Bottom panel: Fluorescence merge (merge of DAPI, membrane, and endosomes) and the merge of the two endosome-labeling channels (eF650 NC-Tf/eF525 NC-Tf). Differential labeling of the two different endosomal compartments is apparent. Note: The NC650-Tf channel is false-colored red.

transferrin (Tf). This protein is commonly used as a surrogate or mediator to facilitate endocytic uptake and delivery of a variety of protein, drug, and nanoparticle cargos to vesicles in the endolysosomal system.[39,40] Interestingly, this was also the first protein ever attached to a hydrophilic semiconductor nanoparticle to facilitate cellular delivery in a similar manner.[1] However, in contrast to simply demonstrating single-color NC uptake, we attempted a two-color labeling of both early and late endosomal vesicles inside the same cells. Understanding how cells endocytose, sort, and recycle numerous different nutrients, metabolites and especially drugs within endosomes continues to be a major basic research goal.[41,42] The photophysical liabilities of conventional organic dyes, including pH sensitivity and susceptibility to photobleaching, coupled with their limiting excitation spectra and red-tailed emission,[32,33] have made such long-term multicolor tracking of these acidified compartments especially challenging.

A549 cells growing as an adherent culture were sequentially labeled with eF525 and eF650 NCs, respectively, preconjugated to human Tf, as described using amine-reactive chemistry (Tf does not contain available cysteine residues for the sulfhydryl-based conjugation). The late endosomes were labeled by incubation of the cells with eF525 NC-Tf (100 nM in complete tissue culture medium) for 12 h. After removal of the conjugates, the cell monolayer was washed and early endosomes were labeled by incubation with eF650 NC-Tf (50 nM in complete tissue culture medium) for 1 h. This same approach has been previously used to label and track NC fate in the endolysosomal system.[43] The cells were subsequently washed, fixed, and blocked with 1% BSA/PBS. As an alternative to the direct labeling protocol described above, the cell membranes were also labeled by incubating the cells with eF565 NC conjugated to anti-human CD61 (integrin β3) antibodies and the nuclei were counterstained with DAPI. Figure 6 shows representative micrographs collected from these cells, including each of the three NC colors, along with DAPI from the nuclei (see Materials and Methods for imaging details). As can be seen, the PL from each NC color yields unique, distinctive labeling with no visible "cross-talk" between them. This is quite remarkable given that the eF525 and eF565 NC probes only have 40 nm separating their emission peaks. More importantly, the clear separation in NC PL from this, and many similar images, allowed us to analyze the relative ratios of endosomes containing either or both NC colors using NIH Image J software. At ~63%, the largest fraction of endosomes appears exclusively green (early eF525 NC), as expected, a much smaller number of ~7% appear exclusively red (late-eF650 NC), with the remaining fraction of ~30% observed in yellow, indicating that both colors of NC (green/red) are present within the same compartment. These ratios are clearly not uniform within each cell, as some cells display high percentages of just one color/NC or both together. Control experiments where eF525 NC-Tf and Cy5-labeled Tf were codelivered to the same cells confirmed that the NCs were indeed located

within endosomes (data not shown). We also probed for potential toxicity in cells exposed to the NC-Tf conjugates and found that viability was essentially unchanged at ~90 ± 10%, similar to previous reports (see Supporting Information).[43]

Overall, these results are consistent with the notion that, depending upon cell-type, dosage, and other complex factors, a significant amount of the NC materials present in late endosomes may be recycled out over time.[13,44] Given the interest in developing nanoparticle-mediated drug delivery, it is clear that the superior NC photophysical properties will provide an important tool to understand the complexity of the underlying processes and how subtle differences either in nanoparticle material or surface bioconjugation can alter delivery site and intracellular residence time.[7,9,45]

DISCUSSION AND CONCLUSIONS

We describe here two related and widely applicable methodologies for NC bioconjugation that show general utility, excellent specificity, and a wide dynamic range for multiplexed fluorescent applications. The bioconjugation chemistries developed over the last 50 years have been the single most significant contributor toward the wide utility of fluorescence techniques in all aspects of biological research and medical diagnostics today.[18,33] Indeed, the ability to obtain almost any organic dye in a "reactive" form and directly couple it to amines or thiols on biomolecules in a relatively facile manner continues to keep these two-related modifications the most popular routes to fluorescent labeling. The NC-conjugation chemistries described here come closest to replicating these approaches. This is not the first application of either chemical strategy with semiconductor NCs. Maleimide groups have been introduced onto NC surfaces using a custom synthesized heterobifunctional amino-maleimide cross-linker.[46] These were then conjugated to sulfhydryl-modified lipids to facilitate high-speed cell surface tracking experiments. A converse approach was also demonstrated where a maleimide-displaying heterobifunctional linker targeted free thiols displayed on the surface of silanized NCs allowing subsequent linkage to aminolated DNA.[47] Peptides and DNA appropriately modified with the cognate groups have also been ligated to both formylbenzoyl and HyNic-modified oligohistidine-appended peptides to facilitate their subsequent self-assembly to NCs in a two-step process.[16] This chemistry was further extended to a one-step/on-NC ligation format.[48] The synthetically intense, multistep preparation previously required to achieve these NC bioconjugations is now negated by NC availability in a preactivated form along with appropriate reagents coupled to rapid, simplified protocols. Importantly, this is also the first time a simple chemical strategy for NC biomolecule ligation has proven to be useful for a broad range of multiplexed fluorescent applications without having to tailor the NCs or ligation chemistry for each.

Control over the orientation of antibody attachment to NCs has always been especially challenging with EDC-based chemistry, which inherently results in heterogeneous display.[20,49,50] Despite this, in almost all the above assays we note a functional equivalence between conjugates assembled using either amine or thiol-targeting chemistries. This suggests that the selective exclusion of the ubiquitous protein (and sometimes NC) carboxyl groups from reactions along with exclusive binding to amines on target antibodies can improve subsequent conjugate activity. The NC-maleimide chemistry, as implemented here, targets the disulfide bridges at the antibody hinge region. This strategy favors attachment of the antibody to the NC, with the active binding region extended outward and still available. The *in situ* reduction greatly simplifies conjugation to only a few minimal steps while also removing the need for purifying antibody fragments prior to NC conjugation. These two chemistries display a high degree of *effective* bioorthogonality in that they (*i*) target only one specific functional group on the proteins, (*ii*) do not have significant, undesirable reactivity toward other functional groups present, (*iii*) provide a well-defined point of attachment between the nanoparticle and the biomolecule, (*iv*) are stable in aqueous solution, (*v*) proceed efficiently without large excesses of either component, and (*vi*) can be achieved within relatively short reaction times.[51,52]

More importantly, these chemistries facilitated multiplexing in all the assay formats in which we applied them, including five-color immunofluorescent imaging of mouse splenic tissue. The examples demonstrated here incorporate from one to five differentially emissive NCs in addition to organic dyes and the DAPI DNA stain. Although not extensively optimized, individual emissions were all clearly resolvable in every case. The availability of multiple widely separated NC emissions in conjunction with orthogonal bioconjugation chemistries and the ability to incorporate further organic/fluorescent protein labels suggest that far higher order or "deep" multiplexing may be readily achievable in diverse fluorescent assay formats while maintaining high sensitivity in a manner similar to previous NC-assay reports.[53] It is quite probable that multiplexed assays incorporating these NCs will be extended to *in vivo* cellular monitoring of complex spaciotemporal processes as well as single molecule and super-resolution microscopy formats.[3,54] We expect both chemistries to be similarly applicable to assembling conjugates and multiplexing with synthetic oligonucleotides. For assays based on immunolabeling, factors limiting target density will remain antibody-cross reactivity, affinity, and the ability to quantitatively resolve closely spaced NC emissions. The ease with which different NC colors can also be used to specifically

and directly label cellular membranes may help facilitate both colocalization studies and multicolor probing strategies. These reactive chemistries can significantly expand the utility of luminescent semiconductor NCs for multiplex formats within many biological applications.

MATERIALS AND METHODS

Immunoassays. *Materials. Staphylococcal enterotoxin* B (SEB) and affinity purified rabbit anti-SEB were purchased from Toxin Technology, Inc. (Sarasota, FL). Rabbit anti-chicken IgG (IgY), chicken IgG, goat anti-mouse IgG, and mouse IgG were purchased from Jackson ImmunoResearch Laboratories, Inc. (West Grove, PA). Phosphate-buffered saline (PBS), Corning Costar flat bottom high binding white 96-well assay plates, Thermal Seal sealing film for 96-well plates and bovine serum albumin (BSA) were obtained from Sigma-Aldrich (St. Louis, MO). Millipore Amicon Ultra centrifugal filter devices, 100 kDa, were purchased from Millipore Corporation (Billerica, MA). eFluor eF525-, eF605-, and eF650-maleimide functionalized nanocrystals (NCs) were prepared and supplied by eBioscience (San Diego, CA). Doubly distilled water (ddH_2O) was used throughout the experiments and was prepared in-house using a Nanopure Diamond water purification system (Barnstead, Dubuque, IA).

Labeling Antibodies with NCs. Antibodies were labeled with the eBioscience eFluor NCs using the sulfhydryl-reactive conjugation reagents and instructions provided by the manufacturer. Briefly lyophilized NCs were reconstituted in 200 μL Conjugation Buffer by heating the mixture on high in a microwave for 5−10 s, repeating 3−4 times as necessary. A total of 200 μg of antibody was then added to the NCs and the reaction incubated for 2 h at RT on a shaker. For the immunoassay triplex studies, eF525-, eF605-, and eF650-maleimide NCs were conjugated to rabbit anti-chicken IgG, goat anti-mouse IgG, and rabbit anti-SEB, respectively. After 2 h, the reaction was stopped by adding 0.7 μL of quencher directly to the mixture, vortexing, and incubating for an additional 10 min on the shaker. The resulting antibody-conjugated NCs were purified using a 100 KDa centrifugal filter unit. The reaction mixture was added to a centrifugal filter unit (pre-equilibrated with purification buffer), and the volume was increased to a total of 1 mL using purification buffer, before being spun at 1000 g for 10 min (Beckman CS-6KR Centrifuge). Once the sample volume had reduced to ~0.1 mL, an additional 1 mL of purification buffer was added and the spin repeated, and this process was repeated for a total of 4 spins. The NC-antibody conjugate was then transferred to a 1.5 mL microcentrifuge tube and spun at 2,500 x g for 5 min to remove any aggregates. The purified NC−antibody conjugate was characterized using UV−visible spectroscopy (Ultrospec 2100 Pro UV/Visible Spectrophotometer GE Healthcare, Piscataway, NJ) and stored at 4 °C prior to use.

Patterning 96-Well Plates with Capture Antibodies. High binding white 96-well assay plates were functionalized with capture antibodies prior to immunoassays. Wells were functionalized with either single capture antibody species, by adding 50 μL per well of 10 μg/mL rabbit anti-chicken IgG, goat anti-mouse IgG, or rabbit anti-SEB in PBS, or multiple capture species, by adding 50 μL of a capture antibody mix in PBS. The capture antibody mix comprised 4 μg/mL rabbit anti-chicken IgG, 4 μg/mL goat anti-mouse IgG, and 2 μg/mL rabbit anti-SEB in PBS. The wells were sealed with Thermal Seal sealing film and incubated for ~1 h at RT and then overnight at 4 °C. The wells were then emptied, washed 4× 200 μL/well with ddH_2O, then filled with 200 μL/well PBS + 1% BSA, and blocked at RT for ~1.5 h on a rocker (The Belly Dancer, Stovall LifeScience, Inc., Greensboro, NC).

Triplex Immunoassay. Following blocking, the blocking solution was removed from the wells and 50 μL/well of the appropriate sample was added. Samples for the triplex immunoassay comprised mixed concentrations of chicken IgG (C: 0−2.5 μg/mL), mouse IgG (M: 0−2.5 μg/mL), and SEB (S: 0−0.5 μg/mL) in PBS + 0.1% BSA. These were left to incubate on a rocker for 1.5 h at RT. The wells were then washed with PBS (4× 200 μL/well) before the tracer mix was added, 50 μL/well, and incubated for 1 h at RT on the shaker. The triplex immunoassay tracer mix consisted of eF525 NC-rabbit anti-chicken IgG (1:10 dilution), eF605 NC-goat anti-mouse IgG (1:20 dilution), and eF650 NC-rabbit anti-SEB (1:100 dilution) NCs in PBS + 0.1% BSA. The wells were then washed with 2× 200 μL/well PBS followed by 2× 200 μL/well ddH_2O and dried with air. The fluorescence intensity and fluorescence intensity wavelength scans were recorded using a Tecan Infinite M1000 Dual Monochromator Multifunction Plate Reader using an excitation of 400 nm (Tecan, Research Triangle Park, NC).

Flow Cytometry Analysis. Human whole blood was obtained from the General Clinical Research Center facility at the Scripps Research Institute with IRB approval, and peripheral blood cells were isolated by FICOLL density gradient centrifugation. Proper precautions were taken for handling blood-borne pathogens. Mouse splenocytes were obtained from spleen harvested from Balb/c mice onsite at eBioscience following standard IACUC handling protocols. Cells were resuspended at 1 × 10^7 cells/mL in eFluor NC Flow Cytometry Staining Buffer and 100 μL of cells were stained as follows: mouse splenocytes were stained with a mixture of anti-CD3 PerCP-eF710 (clone 17A2), anti-CD4 eF605 NC (clone GK1.5), anti-CD45R eF450 (clone RA3−6B2), and anti-CD8a eF660 (clone 53−6.7); normal human peripheral blood cells were stained with a mixture of anti-CD4 APC-eF780 (clone RPA-T4), anti-CD8a eF650 NC (clone RPA-T8), anti-CD19 eF450 (clone HIB19), and anti-CD56 PerCP-eF710 (clone CMSSB). All antibodies were used at the optimal concentration, as determined previously from single-color titration experiments and defined by both low background staining of negatively expressing cells and baseline separation between negatively and positively expressing cells. Cells were stained for 30 min at 2−8 °C, washed by adding 2 mL of eFluor NC Flow Cytometry Staining Buffer, and centrifuged at 500 g for 3 min. The supernatant was discarded and the cells were resuspended in approximately 300 μL of eFluor NC Flow Cytometry Staining Buffer. Data were acquired on an LSR II flow cytometer (Becton Dickenson) using either the 405 nm laser (eF605 NC, eF650 NC, eF450), the 488 nm laser (PerCP-eF710), or the 633 nm laser (eF660, APC-eF780) and analyzed using FlowJo software (Tree Star, Inc.).

Multicolor Cellular Immunocytochemistry. MCF-7 cells were plated onto 8-well chamber slides at a density of ~40,000 cells/well in complete DMEM with 10% FBS, allowed to attach and cultured overnight to 80−90% confluency before fixing with 100% methanol for 10 min at −20 °C. Wells were gently washed with 1X PBS, pH 7.4 for a total of three times, not allowing the well to dry at any time. Nonspecific binding sites were blocked for 1 h at room temperature with 1% BSA in TBS. The blocking solution was removed and combinations of either 2 sulfyhydryl-reactive or 2 amine-reactive NC-conjugated antibodies with the Alexa Fluor 647-conjugated Ki-67 antibody were diluted in the blocking solution and incubated with the cells overnight at 4 °C. The sulfyhydryl-conjugated antibodies were combined together at the following concentrations: 40 nM acidic cytokeratin (clone AE1-eF605 NC), 1 nM tubulin (clone DM1A-eF650 NC), and 5 μg/mL Ki-67 (clone 20Raj1-Alexa Fluor 647). The amine-conjugated antibodies were coupled to the same NCs as were used for the sulfyhydryl products but were used at 20 nM acidic cytokeratin-eF605 NC, 1 nM tubulin-eF650 NC, and 5 μg/mL Ki-67-Alexa Fluor 647. Following incubation, the antibody solutions were aspirated and the wells were washed three times with 1× TBS, pH 7.4. The chambers were removed from the slide and the slides coverslipped with Fluoromount G mounting medium. The edges of the coverglass were sealed with clear nail polish. The fluorescence signal was visualized using a

Zeiss Axiovert 200 epifluorescence microscope equipped with a mercury arc lamp and optimal filter sets for the 605NC, 650NC, and the Alexa Fluor 647 emission wavelengths. Optimal exposure time for each channel was determined and images combined Zeiss Axiovision 4.8 software.

Multicolor Immunohistochemistry of Mouse Spleen Tissue. Male C57BL mice were euthanized using isoflurane followed by cervical dislocation using IACUC-approved protocols. The spleen was removed and placed in ice-cold 1× PBS, pH 7.2, and rapidly frozen in 2-methyl butane on dry ice for 30 s prior to removing and embedding the spleen in OCT compound. The spleen was stored at −80 °C until sectioning. A 10 μm thick section was cut using a Leica CM3000 cryostat, mounted onto Superfrost Plus slide, and stored at −80 °C.

Prior to staining, sections were allowed to come to room temperature, were fixed for 10 min in 100% acetone, and were then gently washed with 1× TBS, pH 7.4. Nonspecific binding sites within the tissue were blocked with 1% BSA in TBS for 1 h at room temperature. Experiments were performed to optimize the concentration of NC-labeled antibodies on sections of spleen after which a cocktail of NC-labeled antibodies was prepared by diluting each of the NC-labeled antibodies to its predetermined optimal concentration. The five NC-labeled antibodies were diluted to the following concentration and combined in 1% BSA TBS as follows: eF525- B220/20nM, eF565-PECAM-1/20nM, eF605-CD11b/5nM, eF625-CD4/5nM, and eF650-CD11c/1nM. Slides were also prepared using each of the NC-labeled antibodies alone as well as one slide with blocking solution and no antibodies to serve as an autofluorescence control. The blocking solution was removed from the section, and the five-color antibody solution (or single colors) was overlaid and covered with Parafilm and incubated in the dark at 4 °C overnight. Sections were washed with three changes of 1× TBS and coverslipped with Fluoromount G mounting medium. The edges of the coverglass were sealed with clear nail polish.

Fluorescence intensity was imaged using an Axiovert 200 microscope equipped with a Nuance EX spectral imager (CRI). All images were taken using a 20× Plan Apochromat objective and using a 460 nm excitation, 475 nm dichroic, and 500 nm long pass emission filter. Images were taken from 500 to 750 nm at 10 nm intervals using an exposure time of 50−100 ms. A spectral library was constructed from the individually stained slides consisting of the representative spectrum of each of the NCs and the autofluorescence signal. By assigning a NC to each representative spectrum and subtracting out the autofluorescence spectrum, the Nuance software was able to differentiate each individual NC signal. The five-color slide was then imaged and each NC spectra identified and assigned a pseudocolor in the combined image shown in Figure 5B.

Labeling of Cell Membranes and *In Vivo* NC Uptake. *Cell Culture.* Human alveolar adenocarcinoma cells (A549, ATCC) were cultured in complete growth medium (Dulbecco's Modified Eagle's Medium, DMEM; purchased from ATCC) supplemented with 1% (v/v) antibiotic/antimycotic and 10% (v/v) heat inactivated fetal bovine serum (ATCC). Cells were cultured in T-25 flasks and incubated at 37 °C under 5% CO_2 atmosphere and a subculture was performed every 3−4 days as described.[1]

Labeling of Cellular Membranes with Maleimide-NCs. We found that when maleimide-activated NCs were subjected to the conjugation procedure, the NCs could be used to efficiently label the cell membranes of fixed cells. A549 cells were seeded onto the wells of Lab-tek chambered coverwell slides (Nunc) that were coated with fibronectin (5 μg/mL in PBS). Cell monolayers were fixed with 3.7% paraformaldehyde, washed with PBS, and blocked with PBS containing 1% bovine serum albumin (1% BSA/PBS) for 1 h at room temperature. Maleimide-eF565, eF605, or eF650 NC solutions (250 nM in 1% BSA/PBS) were incubated on the cells for 1 h. Cells were then washed twice with PBS. Nuclei were counterstained with DAPI (2 μg/mL in PBS).

Conjugation of NCs to Anti-Human CD61 (Integrin β3) Antibody. Conjugation buffer (100 μL) was added to 0.67 nmol maleimide-activated eF565 NCs and incubated in a 60 °C water bath for 10 min to reconstitute the NCs. Anti-human CD61 (1.0 nmol; integrin β3) in phosphate buffered saline (PBS) was added to the NCs, and the conjugation reaction was stirred at room temperature for 2 h. Unreacted maleimide groups on the NCs were quenched by adding 0.7 μL of quenching buffer, and the conjugate was purified using a desalting column. As a negative control, NCs were subjected to the bioconjugation procedure in the absence of antibody.

Conjugation of NCs to Transferrin. Human holo-transferrin (Tf) was purchased from Sigma-Aldrich. All other reagents and materials were obtained from eFluor Nanocrystal Conjugation Kit - Amine-Reactive. Solid Tf was dissolved in 100 μL 1× PBS, pH 7.4 (concentration 13.3 μM), and mixed with 1.6 μL sulfo-HyNic solution (10 mg/mL stock in DMF). The reaction was mixed at room temperature for 2 h. The protein solution was added to a ProSpin column (pre-equilibrated with 650 μL of conjugation buffer for at least 30 min and spun at 750 g for 2 min to remove excess buffer) and centrifuged at 750 g for 2 min. The resulting filtrate was added to 4FB modified eF650 NC solution (0.67 nmoles) with 13 μL of aniline buffer solution. The reaction was shaken for 2 h. Prior to reaction completion, 5.2 mg 2-sulfobenzaldehyde was dissolved into 50 μL of conjugation buffer to yield the quenching solution. A volume of 10 μL of quenching solution was added to the reaction mixture and the mixture was shaken for an additional 10 min. The reaction was then added to a 100k MWCO concentrator (pre-equilibrated with 1 mL of purification buffer) and diluted to 1−3 mL total volume. The concentrator was spun at 3000 rpm for 10 min and the effluent was discarded. Dilution and concentration was repeated for a total of four concentration steps. The residual reaction solution was transferred to a microcentrifuge tube and spun at 7000 rpm for 5 min to remove any precipitation/aggregates. The supernatant was isolated and stored at 4 °C. NC concentration was determined through UV−vis absorption analysis ($\varepsilon_{645\ nm} = 1.11 \times 10^6\ M^{-1}\ cm^{-1}$).

Multicolor Cellular Labeling. Live A549 cells were labeled sequentially with eF525 and eF650 NCs conjugated to human transferrin (Tf) to label the late and early endosomes, respectively. Late endosomes were labeled by the incubation of the cells with eF525 NC-Tf (100 nM in complete tissue culture medium) for 12 h. After removal of the conjugates, the cell monolayer was washed and early endosomes were labeled by incubation of the cells with eF650 NC-Tf (50 nM in complete tissue culture medium) for another 12 h. The cells were washed, fixed, and blocked with 1% BSA/PBS. The cell membrane was labeled by incubation of the cells with the anti-human CD61-eF565 NC conjugate (200 nM in 1% BSA/PBS) overnight at 4 °C. Nuclei were stained with DAPI (2 μg/mL in PBS).

Microscopy. Epifluorescence image collection was carried out using an Olympus IX-71 microscope where samples were excited with a Xe lamp. Differential interference contrast (DIC) images were collected using a bright light source. Filter cubes utilized are shown in Supporting Information, Table 1. Micrographs were captured with a DP71 color digital camera (Olympus, Center Valley, PA) using constant camera settings over time, as indicated. Images were analyzed using DP Manager Software (Olympus, Center Valley, PA) and Image J (NIH, Bethesda, MD; http://rsb.info.nih.gov/ij/).

Acknowledgment. The authors acknowledge the CB Directorate/Physical S&T Division (DTRA), DARPA, ONR, NRL, and the NRL-NSI for financial support. K.B. and D.P. acknowledge ASEE fellowships through NRL. K.S. and S.S. acknowledge the Critical Path Initiative FDA for financial support. T.L.J. is grateful to Drs. M. Fung and C. Funatake for helpful discussions and interpretations in flow cytometry. W.R.A. is grateful to the Natural Sciences and Engineering Research Council of Canada (NSERC) for support through a postdoctoral fellowship.

Disclaimer: The mention of commercial products, their sources, or their use in connection with material reported herein is not to be construed as either an actual or implied endorsement of such products by the Department of Health and Human Services.

Supporting Information Available: Supporting images for the immunoassays and flow cytometry. List of filter cubes for the microscopy and cell viability assay data. Description of DLS and HR-TEM analysis and additional control/supporting data. This

material is available free of charge *via* the Internet at http://pubs.acs.org.

REFERENCES AND NOTES

1. Chan, W. C. W.; Nie, S. Quantum Dot Bioconjugates for Ultrasensitive Nonisotopic Detection. *Science* **1998**, *281*, 2016–2018.
2. Bruchez, M., Jr.; Moronne, M.; Gin, P.; Weiss, S.; Alivisatos, A. P. Semiconductor Nanocrystals as Fluorescent Biological Labels. *Science* **1998**, *281*, 2013–2016.
3. Kim, B. Y. S.; Rutka, J. T.; Chan, W. C. W. Nanomedicine. *New Engl. J. Med* **2010**, *363*, 2434–2443.
4. Baker, M. Nanotechnology Imaging Probes:Smaller and More Stable. *Nat. Methods* **2010**, *7*, 957–961.
5. Pinaud, F.; Clarke, S.; Sittner, A.; Dahan, M. Probing Cellular Events, One Quantum Dot at a Time. *Nat. Methods* **2010**, *7*, 275–285.
6. Kim, S.; Lim, Y. K.; Soltesz, E. G.; De Grand, A. M.; Lee, J.; Nakayama, A.; Parker, J. A.; Mihaljevic, T.; Laurence, R. G.; Dor, D. M.; Cohn, L. H.; Bawendi, M. G.; Frangioni, J. V. Near-Infrared Fluorescent Type II Quantum Dots for Sentinel Lymph Node Mapping. *Nat. Biotechnol.* **2004**, *22*, 93–97.
7. Wong, C.; Stylianopoulos, T.; Cui, J.; Martin, J.; Chauhan, V. P.; Jiang, W.; Popovic, Z.; Jain, R. K.; Bawendi, M. G.; Fukumura, D. Multistage Nanoparticle Delivery System for Deep Penetration into Tumor Tissue. *Proc. Natl. Acad. Sci. U.S.A.* **2011**, *108*, 2426–2431.
8. Juzenas, P.; Chen, W.; Sun, Y. P.; Coelho, M. A.; Generalov, R.; Generalova, N.; Christensen, I. L. Quantum Dots and Nanoparticles for Photodynamic and Radiation Therapies of Cancer. *Adv. Drug Delivery Rev.* **2008**, *60*, 1600–1614.
9. Delehanty, J. B.; Boeneman, K.; Bradburne, C. E.; Robertson, K.; Medintz, I. L. Quantum Dots: a Powerful Tool for Understanding the Intricacies of Nanoparticle-Mediated Drug Delivery. *Exp. Opin. Drug Delivery* **2009**, *6*, 1091–1112.
10. Algar, W. R.; Krull, U. J. New Opportunities in Multiplexed Optical Bioanalyses using Quantum Dots and Donor-Acceptor Interactions. *Anal. Bioanal. Chem.* **2010**, *398*, 2439–2449.
11. Resch-Genger, U.; Grabolle, M.; Cavaliere-Jaricot, S.; Nitschke, R.; Nann, T. Quantum Dots Versus Organic Dyes as Fluorescent Labels. *Nat. Methods* **2008**, *5*, 763–775.
12. Rogach, A. L.; Ogris, M. Near-Infrared-Emitting Semiconductor Quantum Dots for Tumor Imaging and Targeting. *Curr. Opin. Mol. Ther.* **2010**, *12*, 331–339.
13. Biju, V.; Itoh, T.; Ishikawa, M. Delivering Quantum Dots to Cells: Bioconjugated Quantum Dots for Targeted and Nonspecific Extracellular and Intracellular Imaging. *Chem. Soc. Rev.* **2010**, *39*, 3031–3056.
14. Han, H. S.; Devaraj, N,K.; Lee, J.; Hilderbrand, S. A.; Weissleder, R.; Bawendi, M. G. Development of a Bioorthogonal and Highly Efficient Conjugation Method for Quantum Dots Using Tetrazine-Norbornene Cycloaddition. *J. Am. Chem. Soc.* **2010**, *132*, 7838–7839.
15. Genin, E.; Carion, O.; Mahler, B.; Dubertret, B.; Arhel, N.; Charneau, P.; Doris, E.; Mioskowski, C. CrAsH-Quantum Dot Nanohybrids for Smart Targeting of Proteins. *J. Am. Chem. Soc.* **2008**, *130*, 8596–8597.
16. Prasuhn, D. E.; Blanco-Canosa, J. B.; Vora, G. J.; Delehanty, J. B.; Susumu, K.; Mei, B. C.; Dawson, P. E.; Medintz, I. L. Combining Chemoselective Ligation with Polyhistidine Driven Self-Assembly for the Modular Display of Biomolecules on Quantum Dots. *ACS Nano* **2010**, *4*, 267–278.
17. Dif, A.; Boulmedais, F.; Pinot, M.; Roullier, V.; Baudy-Floc'h, M.; Coquelle, F. M.; Clarke, S.; Neveu, P.; Vignaux, F.; Le Borgne, R.; et al. Small and Stable Peptidic PEGylated Quantum Dots to Target Polyhistidine-Tagged Proteins with Controlled Stoichiometry. *J. Am. Chem. Soc.* **2009**, *131*, 14738–14746.
18. Hermanson, G. T. Bioconjugate Techniques. 2008 Second ed. Academic Press, San Diego; 2008.
19. Klostranec, J. M.; Chan, W. C. W. Quantum Dots in Biological and Biomedical Research: Recent Progress and Present Challenges. *Adv. Mater.* **2006**, *18*, 1953–1964.
20. Medintz, I.; Uyeda, H.; Goldman, E.; Mattoussi, H. Quantum Dot Bioconjugates for Imaging, Labeling and Sensing. *Nat. Mater.* **2005**, *4*, 435–446.
21. Pereira, M.; Lai, E. P. Capillary Electrophoresis for the Characterization of Quantum Dots After Non-Selective or Selective Bioconjugation with Antibodies for Immunoassay. *J. Nanobiotechnol.* 2008, *6*, doi:10.1186/1477-3155-1186-1110.
22. Sapsford, K. E.; Pons, T.; Medintz, I. L.; Higashiya, S.; Brunel, F. M.; Dawson, P. E.; Mattoussi, H. Kinetics of Metal-Affinity Driven Self-Assembly Between Proteins or Peptides and CdSe-ZnS Quantum Dots. *J. Phys. Chem. C* **2007**, *111*, 11528–11538.
23. Peng, Z. A.; Peng, X. Nearly Monodisperse and Shape-Controlled CdSe Nanocrystals *via* Alternative Routes: Nucleation and Growth. *J. Am. Chem. Soc.* **2002**, *124*, 3343–3353.
24. Dubertret, B.; Skourides, P.; Norris, D. J.; Noireaux, V.; Brivanlou, A. H.; Libchaber, A. In Vivo Imaging of Quantum Dots Encapsulated in Phospholipid Micelles. *Science* **2002**, *298*, 1759–1762.
25. Dirksen, A.; Dawson, P. E. Rapid Oxime and Hydrazone Ligations with Aromatic Aldehydes for Biomolecular Labeling. *Bioconjugate Chem.* **2008**, *19*, 2543–2548.
26. Dirksen, A.; Hackeng, T. M.; Dawson, P. E. Nucleophilic Catalysis of Oxime Ligation. *Angew. Chem., Int. Ed.* **2006**, *118*, 7743–7746.
27. Tiefenbrunn, T. K.; Dawson, P. E. Chemoselective Ligation Techniques: Modern Applications of Time-Honored Chemistry. *Biopolymers* **2010**, *94*, 95–106.
28. Hartwell, S. K.; Grudpan, K. Flow Based Immuno/Bioassay and Trends in Micro-Immuno/Biosensors. *Microchim. Acta* **2010**, *169*, 201–220.
29. Ng, A. H. C.; Uddayasankar, U.; Wheeler, A. R. Immunoassays in Microfluidic Systems. *Anal. Bioanal. Chem.* **2010**, *397*, 991–1007.
30. Ngom, B.; Guo, Y. C.; Wang, X. L.; Bi, D. R. Development and Application of Lateral Flow Test Strip Technology for Detection of Infectious Agents and Chemical Contaminants: a Review. *Anal. Bioanal. Chem.* **2010**, *397*, 1113–1135.
31. Fu, Q.; Schoenhoff, F. S.; Savage, W. J.; Zhang, P. B.; Van Eyk, J. E. Multiplex Assays for Biomarker Research and Clinical Application: Translational Science Coming of Age. *Proteom. Clin. Appl.* **2010**, *4*, 271–284.
32. Sapsford, K. E.; Berti, L.; Medintz, I. L. Materials for Fluorescence Resonance Energy Transfer:Beyond Traditional 'Dye to Dye' Combinations. *Angew. Chem., Int. Ed.* **2006**, *45*, 4562–4588.
33. Haugland, R. P. The Handbook A Guide to Fluorescent Probes and Labeling Technologies, 10th ed.; Invitrogen: San Diego, 2005.
34. Goldman, E. R.; Clapp, A. R.; Anderson, G. P.; Uyeda, H. T.; Mauro, J. M.; Medintz, I. L.; Mattoussi, H. Multiplexed Toxin Analysis Using Four Colors of Quantum Dot Fluororeagents. *Anal. Chem.* **2004**, *76*, 684–688.
35. Medintz, I. L.; Farrell, D.; Susumu, K.; Trammell, S. A.; Deschamps, J. R.; Brunel, F. M.; Dawson, P. E.; Mattoussi, H. Multiplex Charge Transfer Interactions Between Quantum Dots and Peptide-Bridged Ruthenium Complexes. *Anal. Chem.* **2009**, *81*, 4831–4839.
36. Chattopadhyay, P. K.; Price, D. A.; Harper, T. F.; Betts, M. R.; Yu, J.; Gostick, E.; Perfetto, S. P.; Goepfert, P.; Koup, R. A.; De Rosa, S. C.; et al. Quantum Dot Semiconductor Nanocrystals for Immunophenotyping by Polychromatic Flow Cytometry. *Nat. Med.* **2006**, *12*, 972–977.
37. Marjoniemi, V. M. Immunohistochemistry in Gynaecological Pathology: A Review. *Pathology* **2004**, *36*, 109–119.
38. Molnar, B.; Sipos, F.; Galamb, O.; Tulassay, Z. Molecular Detection of Circulating Cancer Cells - Role in Diagnosis, Prognosis and Follow-up of Colon Cancer Patients. *Dig. Dis.* **2003**, *21*, 320–325.
39. Choi, C. H. J.; Alabi, C. A.; Webster, P.; Davis, M. E. Mechanism of Active Targeting in Solid Tumors with Transferrin-Containing Gold Nanoparticles. *Proc. Natl. Acad. Sci. U.S.A.* **2010**, *107*, 1235–1240.

40. Delehanty, J. B.; Mattoussi, H.; Medintz, I. L. Delivering Quantum Dots into Cells: Strategies, Progress and Remaining Issues. *Anal. Bioanal. Chem.* **2009**, *393*, 1091–1105.
41. Ziello, J. E.; Huang, Y.; Jovin, I. S. Cellular Endocytosis and Gene Delivery. *Mol. Med.* **2010**, *16*, 222–229.
42. Rajendran, L.; Knolker, H. J.; Simons, K. Subcellular Targeting Strategies for Drug Design and Delivery. *Nat. Rev. Drug Discovery* **2010**, *9*, 29–42.
43. Delehanty, J. B.; Bradburne, C. E.; Boeneman, K.; Susumu, K.; Farrell, D.; Mei, B. C.; Blanco-Canosa, J. B.; Dawson, G.; Dawson, P. E.; Mattoussi, H.; Medintz, I. L. Delivering Quantum Dot-Peptide Bioconjugates to the Cellular Cytosol: Escaping from the Endolysosomal System. *Integr. Biol.* **2010**, *2*, 265–277.
44. Tekle, C.; van Deurs, B.; Sandvig, K.; Iversen, T. G. Cellular Trafficking of Quantum Dot-Ligand Bioconjugates and Their Induction of Changes in Normal Touting of Unconjugated Ligands. *Nano Lett.* **2008**, *8*, 1858–1865.
45. Shi, J.; Votruba, A. R.; Farokhzad, O. C.; Langer, R. Nanotechnology in Drug Delivery and Tissue Engineering: From Discovery to Applications. *Nano Lett.* **2010**, *10*, 3223–3230.
46. Murcia, M. J.; Minner, D. E.; Mustata, G. M.; Ritchie, K.; Naumann, C. A. Design of Quantum Dot-Conjugated Lipids for Long-Term, High-Speed Tracking Experiments on Cell Surfaces. *J. Am. Chem. Soc.* **2008**, *130*, 15054–15062.
47. Parak, W. J.; Gerion, D.; Zanchet, D.; Woerz, A. S.; Pellegrino, T.; Micheel, C. M.; Williams, S. C.; Seitz, M.; Bruehl, R. E.; Bryant, Z.; et al. Conjugation of DNA to Silanized Colloidal Semiconductor Nanocrystalline Quantum Dots. *Chem. Mater.* **2002**, *14*, 2113–2119.
48. Blanco-Canosa, J. B.; Medintz, I. L.; Farrell, D.; Mattoussi, H.; Dawson, P. E. Rapid Covalent Ligation of Fluorescent Peptides to Water Solubilized Quantum Dots. *J. Am. Chem. Soc.* **2010**, *132*, 10027–10033.
49. Medintz, I. Universal Tools for Biomolecular Attachment to Surfaces. *Nat. Mater.* **2006**, *5*, 842–842.
50. Aubin-Tam, M. E.; Hamad-Schifferli, K. Structure and Function of Nanoparticle-Protein Conjugates. *Biomed. Mater.* 2008, *3*, Article # 034001.
51. Algar, W. R.; Prasuhn, D. E.; Stewart, M.; Jennings, T. L.; Blanco-Canosa, J. B.; Dawson, P.; Medintz, I. L. The Controlled Display of Biomolecules on Nanoparticles: A Challenge Suited to Bioorthogonal Chemistry. *Bioconj. Chem.* **2011**, *22*, 825–858.
52. Sletten, E. M.; Bertozzi, C. R. Bioorthogonal Chemistry: Fishing for Selectivity in a Sea of Functionality. *Angew. Chem., Int. Ed.* **2009**, *48*, 6974–6998.
53. Geissler, D.; Charbonnière, L.; Ziessel, R.; Butlin, N.; Löhmannsröben, H.-G.; Hildebrandt, N. Quantum Dot Biosensors for Ultrasensitive Multiplexed Diagnostics. *Angew. Chem., Int. Ed.* **2010**, *49*, 1396–1401.
54. Patterson, G.; Davidson, M.; Manley, S.; Lippincott-Schwartz, J. Superresolution Imaging Using Single-Molecule Localization. *Annu. Rev. Phys. Chem.* **2010**, *61*, 345–367.